Available online at www.sciencedirect.com

ScienceDirect

Procedia Materials Science 8 (2015) 968 – 977

Procedia Materials Science

www.elsevier.com/locate/procedia

International Congress of Science and Technology of Metallurgy and Materials, SAM - CONAMET 2013

Evolution of Metallographic Parameters during Horizontal Unidirectional Solidification of Zn-Sn Alloys

Wilky Desrosin[a], Lucía Boycho[a], Verónica Scheiber[a], Claudia Marcela Méndez[a], Carlos Enrique Schvezov[a,b], Alicia Esther Ares[a,b,*]

[a]*Faculty of Sciences, University of Misiones, 1552 Félix de Azara Street, 3300 Posadas-Misiones, Argentina.*
[c]*Member of CIC of the National Science Research Council of Argentina (CONICET).*

Abstract

In the present research the horizontal directional solidification of Zn-Sn alloys (Zn-4wt.%Sn, Zn-6wt.%Sn, Zn-10wt.%Sn and Zn-30wt.%Sn) was carried out by extracting heat in two opposite directions. For this purpose, ceramic molds, a muffle, a horizontal furnace with two heat extraction systems at the ends, a measurement, acquisition and recording temperature system, eight K-type thermocouples and an electronic recorder were used. The main parameters involved in the columnar-to-equiaxed transition, CET, were: the moment of start and end of solidification at each position under consideration, cooling rates, the average temperature gradients and critical temperature gradients at the CET. Also, metallographic parameters evolution (secondary dendritic arm spacing) was analyzed in function of the position in the sample and correlated with thermal parameters. The values of the critical thermal gradients for each composition were 0.01 °C/cm (right side) and 0.23 °C/cm (left side) for Zn-4wt%Sn, 0.25 °C/cm (right side) and 0.41 °C/cm (left side) for Zn-6wt%Sn, 1.4 °C/cm (right side) and 1.7 °C/cm (left side) for Zn-10wt%Sn and -0.05 °C/cm (right side) and 0.15 °C/cm (left side) for Zn-30wt%Sn.

Selection and peer-review under responsibility of the scientific committee of SAM - CONAMET 2013

Keywords: Unidirectional solidification; Zn-Sn alloys; thermal parameter evolution, secondary dendritic arm spacings.

* Corresponding author. Tel.: +0054-376-4422186-156; fax: +0054-376-4425414.
E-mail address: aares@fceqyn.unam.edu.ar

Selection and peer-review under responsibility of the scientific committee of SAM - CONAMET 2013
doi:10.1016/j.mspro.2015.04.158

1. Introduction

Solidification of metal alloys, which starts in the external equiaxed region (chill), results in two basic types of structures in a single solidified alloy sample: columnar and equiaxed. The presence of both structures indicates the occurrence of the columnar-to-equiaxed transition phenomenon (Spittle 2006, Gueijman et al. 2010).

Studying the columnar-to-equiaxed transition, CET, is of great technological interest for the evaluation and design of the mechanical properties of the solidification products. To this end, it is necessary to understand the mechanisms by which it occurs. As found in previous studies (Hunt 1984, Ziv and Weinberg 1989, Ares and Schvezov 2000, Ares et al. 2002, Ares et al. 2005, Ares and Schvezov 2007, Gandin 2000, Gandin 2000, Reinhart et al. 2005, Spittle 2006, Yasuda et al. 2006, Mc Fadden et al. 2009, Gueijman et al. 2010), the CET occurs by competition between columnar and equiaxed growth. It is mainly controlled by the parameters of casting, such as the alloy composition, the density of the nuclei present in the liquid, the cooling capacity of the metal / mold, and the degree of convection in the liquid (Spittle 2006).

The aim of the present work is to solidify Zn-Sn alloys of different compositions (Zn-4wt.%Sn, Zn-6wt.%Sn, Zn-10wt.%Sn and Zn-30wt.%Sn) horizontally and directionally, and analyze the evolution of the thermal parameters with the microstructures obtained. The importance of analyzing the dendritic growth is the relation with micro-segregation and other defects.

2. Experimental details

The Zn-4wt%Sn, Zn-6wt.%Sn, Zn-10wt.%Sn and Zn-30wt.%Sn alloy samples were horizontally solidified. Initially the melt was allowed to reach the selected temperature and then, the furnace power was turned off and the melt was allowed to solidify from the bottom. Ceramic molds of 50 mm in diameter, cooled from both ends, were used for horizontal solidification experiments. Eight made K-type thermocouples were used in the experimental setup. For the horizontal setup, thermocouples were fabricated with thin chromel-alumel wires of 0.5 mm diameter that were inserted into bifilar ceramics of 4.0 mm external diameter and 1.0 mm hollow diameter and introduced inside Pyrex® glass rods of 7.0 mm external diameter and a5.3 mm internal diameter.

Adjacent thermocouples were located at a distance of 20 mm. Temperatures were measured at regular intervals of 10 seconds. The horizontal experimental device is shown in Figure 1. Small 140 mm long hemicylindrical probes of Zn-Sn alloy were solidified in the horizontal setup. The heat flux toward the ends of the sample was obtained by two cooling systems located at the ends of the ceramic crucible. In this setup, temperatures at eight different positions were measured using a TC 7003C acquisition system and recorded using SensorWatch® software every 1 minute in a compatible PC from the early beginning until the end of the solidification. Alloys were prepared with high purity metals (electrolytic Zinc and commercial grade Tin). For the horizontal setup, a set of five specimens of each alloy concentration were prepared. The alloy was first melted and mixed in a graphite crucible using a conventional furnace and then poured into a previously heated ceramic crucible. The crucible with the alloy was located into the horizontal furnace and heated up above the melting point of the alloy. The solidification of the sample was obtained by cooling down the alloy using a cooling system which extracts the heat toward both ends (Figure 1).The temperature profiles were determined from the measurements during solidification at the different thermocouple positions and following the phase diagram in Figure 2. The temperature versus time curves for all experiments are presented in Figure 3. Thermocouple T1and T8 are the first to reach the solidification front. From the temperatures versus time graphs it is possible to calculate the cooling velocity in the melt, $\dot{T}$. The velocity associated to each experiment is the average value of the slopes determined from the graphs. The start and the end of solidification at each thermocouple determine the positions of the solidification front versus time, which correspond to the liquidus and the solidus temperature, respectively. Both points are detected by the changes in the slopes of the cooling curve at the start and end of solidification.

This criterion was chosen in order to allow for undercooling to occur before solidification and possible recalescence during solidification of equiaxed grains, since this process is characterized by nucleation and solidification of grains in the melt rather than for what is observed in a normal solidification process where there is a dendrite tip front advancing in the melt. The local solidification time at each thermocouple site is determined by the period of time taken for the temperature to go from the liquidus to the solidus temperature.

The velocity of the liquidus solidification front is calculated as the distance between thermocouples divided by the time taken by the liquidus temperature to go from the lower to the upper thermocouple. These velocities are named as V_L for the liquidus velocity.

The liquid thermal gradient, G_L, at all times is calculated straightforward, dividing the temperature difference between two thermocouples by the separation distance between them.

After solidification, the samples were cut in a longitudinal direction, polished with emery paper and etched to reveal the structure. The reagent used was a solution of HCl acid (70%) during 120 seconds [6]. A solution containing 5 g CrO_3, 0.5 g Na_2SO_4 and 100 ml H_2O (Palmerston´s reagent) was used to reveal the microstructure. The etching time varied from 15 to 20 s, depending on the alloy solute content. After etching, the samples were rinsed in a solution of 20 g CrO_3 and 100 ml H_2O before optical microscopy examination using SEM and an optical microscope in order to measure the average grain size. Typical resulting macrographs and micrographs can be seen in Figure 3. The measurements of spacings were done using the line intersect technique, preferentially in regions near the thermocouple positions for a closer correlation with the solidification parameters.

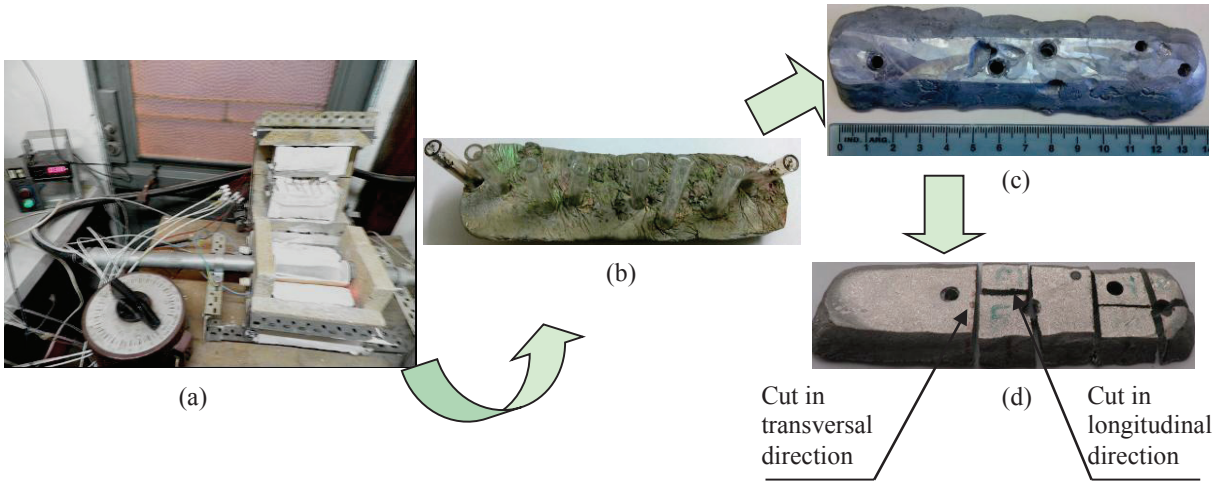

Fig. 1. (a) Directional solidification device. (b) Sample after the experiment showing the positions of eight thermocouples during the test (inside the Pyrex tubes). (c) Macrostructure of pure Zn. (d) Detail of cutting of sample for microstructure observations (in longitudional and transversal directions).

3. Results and Discussion

3.1. Columnar-to-equiaxed transition

A number of four directional solidification experiments in a range of alloy compositions between Zn-4wt.%Sn and Zn-30wt.%Sn were performed. The columnar-to-equiaxed transition phenomenon was obtained in the samples as can be observed in Figures 2 (a) and (b) for two compositions. Due to the heat, extraction was produced in two opposite directions in each sample; two zones of CET were presented. In Table 1 the positions of two CET in each sample are accessible.

Table 1. Positions of both CET in each sample.

Alloy composition	$CET_{Minimum}$(left) (cm)	$CET_{Maximum}$ (right) (cm)	$CET_{Minimum}$(left) (cm)	$CET_{Maximum}$ (right) (cm)
Zn	2.4	4.1	6.5	8.6
Zn-4wt.%Sn	2.2	3.6	8.8	10.5
Zn-6wt.%Sn	1.8	2.7	9.4	11.1
Zn-10wt.%Sn	1.5	2.2	10.6	11.9
Zn-30wt.%Sn	0.9	1.6	11.7	12.2

Observing the values of CET positions in Table 1 it is possible to appreciate that when the concentration of Sn increases the CET occurs before. This could be due to the heat removal efficiency of the cooling system and because the thermal conductivity of Zn (116 W/m.K) is much higher than that of Sn (66.6 W/m.K).

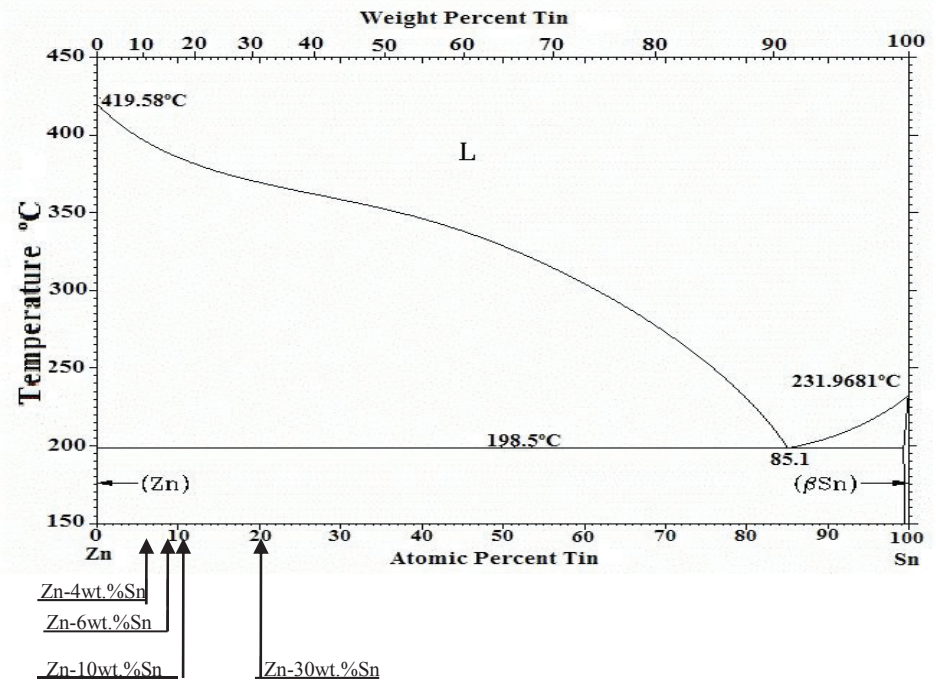

Fig. 2. Zn-Sn phase diagram showing the compositions used in the present research (in weight percent).

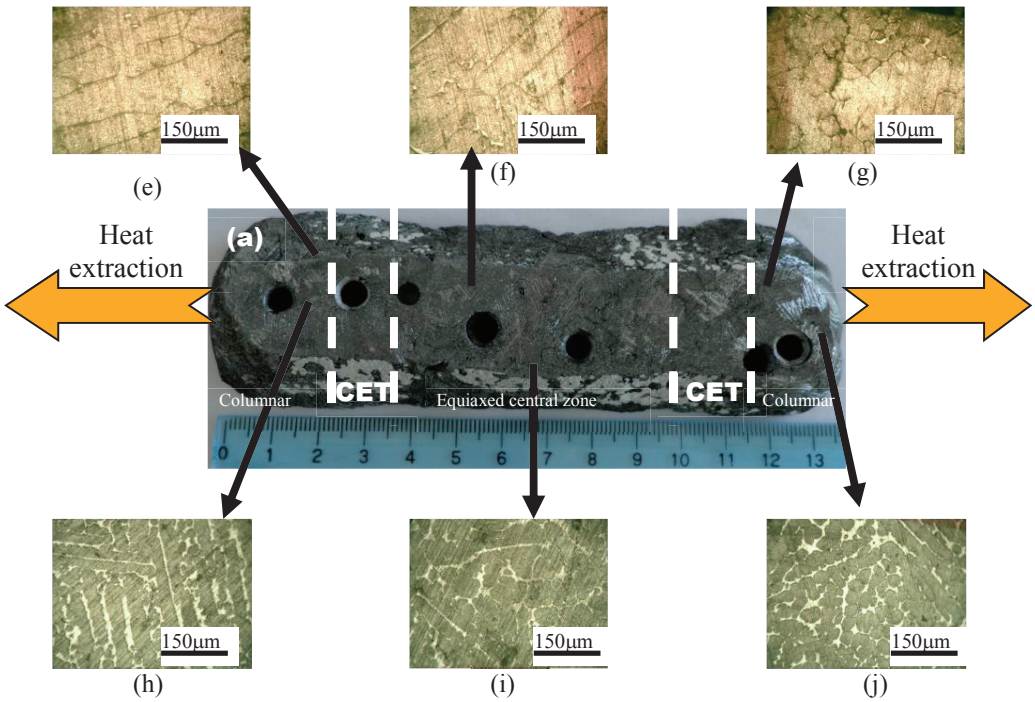

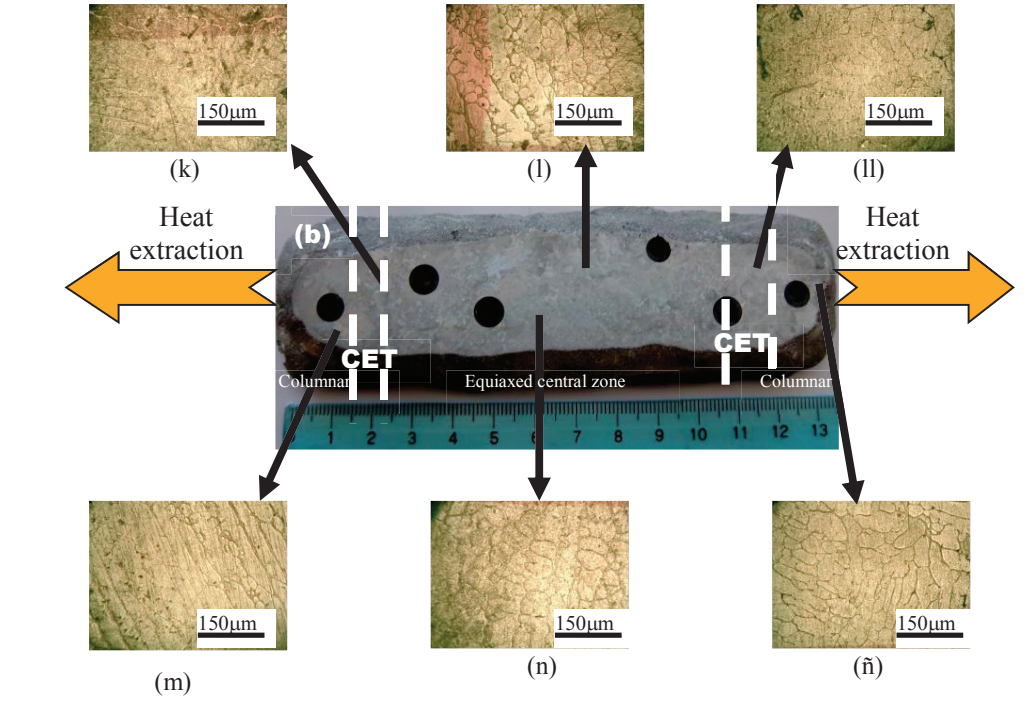
150µm
(k)
150µm
(l)
150µm
(ll)
Heat extraction
(b)
CET
Columnar
Equiaxed central zone
CET
Columnar
Heat extraction
150µm
(m)
150µm
(n)
150µm
(ñ)

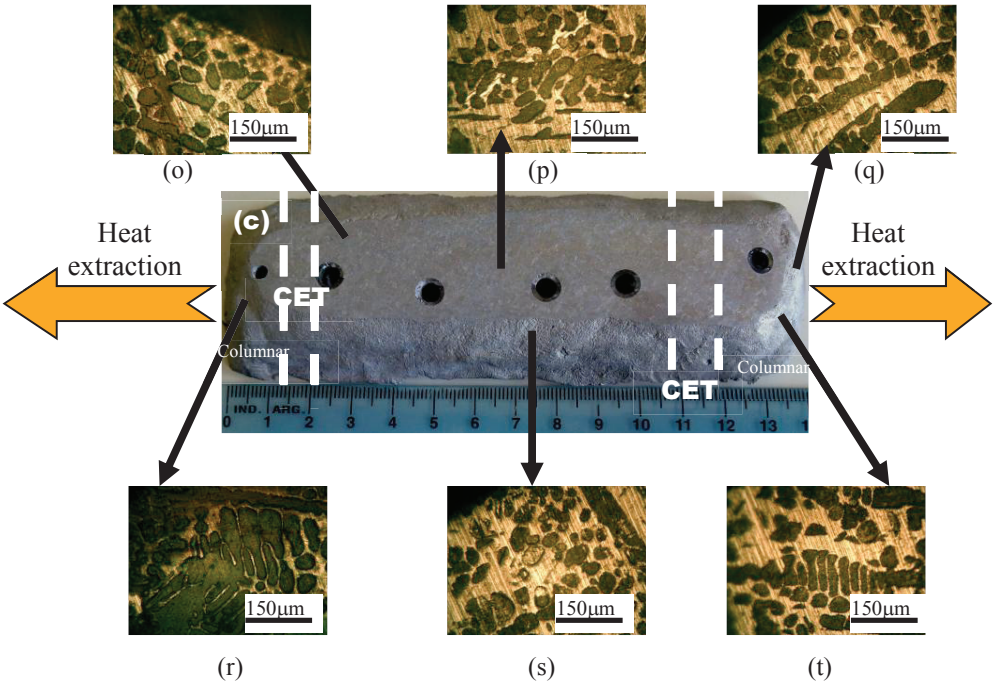
150µm
(o)
150µm
(p)
150µm
(q)
Heat extraction
(c)
CET
Columnar
CET
Columnar
Heat extraction
150µm
(r)
150µm
(s)
150µm
(t)

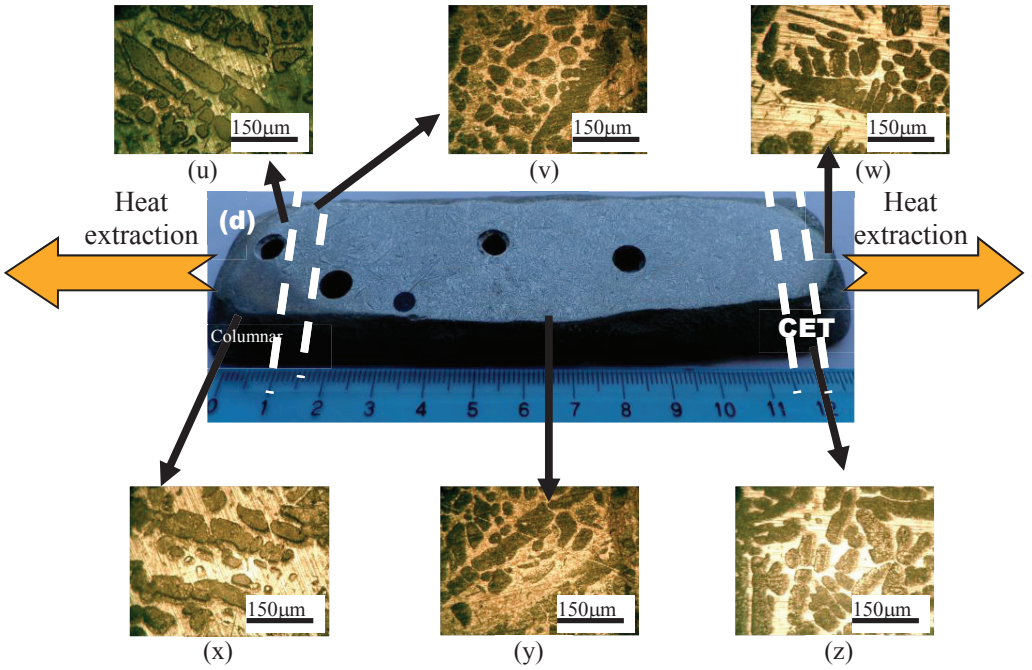

Fig. 3. (a), (b), (c) and (d) Representative macrostructures of Zn-4wt.%Zn, Zn-6wt.%Sn, Zn-10wt.%Sn and Zn-30wt.%Sn alloys. (e) to (z) Microstructures of different zones (columnar, CET and equiaxed) of each sample.

3.2. *Cooling curves and thermal parameters evolution*

Temperature versus time curves for Zn-4wt.%Sn, Zn-6wt.%Al, Zn-10wt.%Al and Zn-30wt.%Sn alloys concentrations are presented in Figure 4. The thermocouples T_1 and T_8 are the first to reach the solidification fronts in both sides of samples. From the temperatures versus time graphs it is possible to calculate the cooling velocity in the melt $\dot{T}$. The velocity associated to each experiment is the average value of the slopes determined from the graphs. The start and the end of solidification at each thermocouple determine the positions of the solidification fronts versus time, which correspond to the liquidus and solidus temperatures, respectively. Both points are detected by changes in the slopes of the cooling curves at the start and end of solidification, as can be seen in Figures 5.

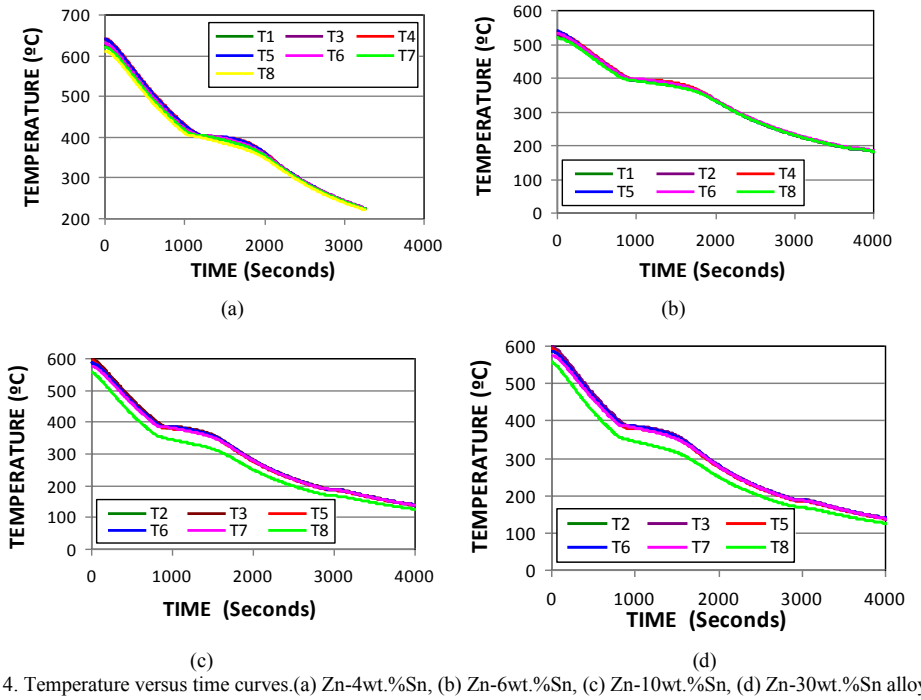

Fig. 4. Temperature versus time curves.(a) Zn-4wt.%Sn, (b) Zn-6wt.%Sn, (c) Zn-10wt.%Sn, (d) Zn-30wt.%Sn alloys.

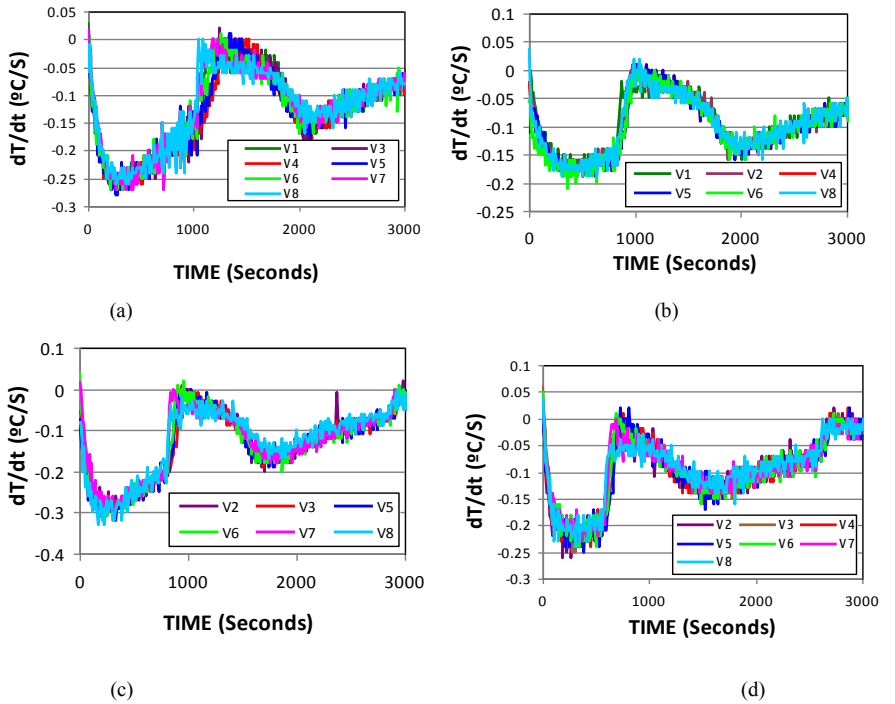

Fig. 5. Cooling rate versus time: (a) Zn-4wt.%Sn, (b) Zn-6wt.%Sn, (c) Zn-10wt.%Sn, (d) Zn-30wt.%Sn alloys.

The values of temperature gradients are plotted in Figure 6 from both ends of the samples where the CET occurs. The minimum value always corresponds to the position of the change of the structure and that is the position of the columnar to equiaxed transition, CET. The values of the critical gradients for each composition were: 0.01 °C/cm (right side) and 0.23 °C/cm (left side) for Zn-4wt%Sn, 0.25 °C/cm (right side) and 0.41 °C/cm (left side) for Zn-6wt%Sn, 1.4 °C/cm (right side) and 1.7 °C/cm (left side) for Zn-10wt%Sn and -0.05 °C/cm (right side) and 0.15 °C/cm (left side) for Zn-30wt%Sn.

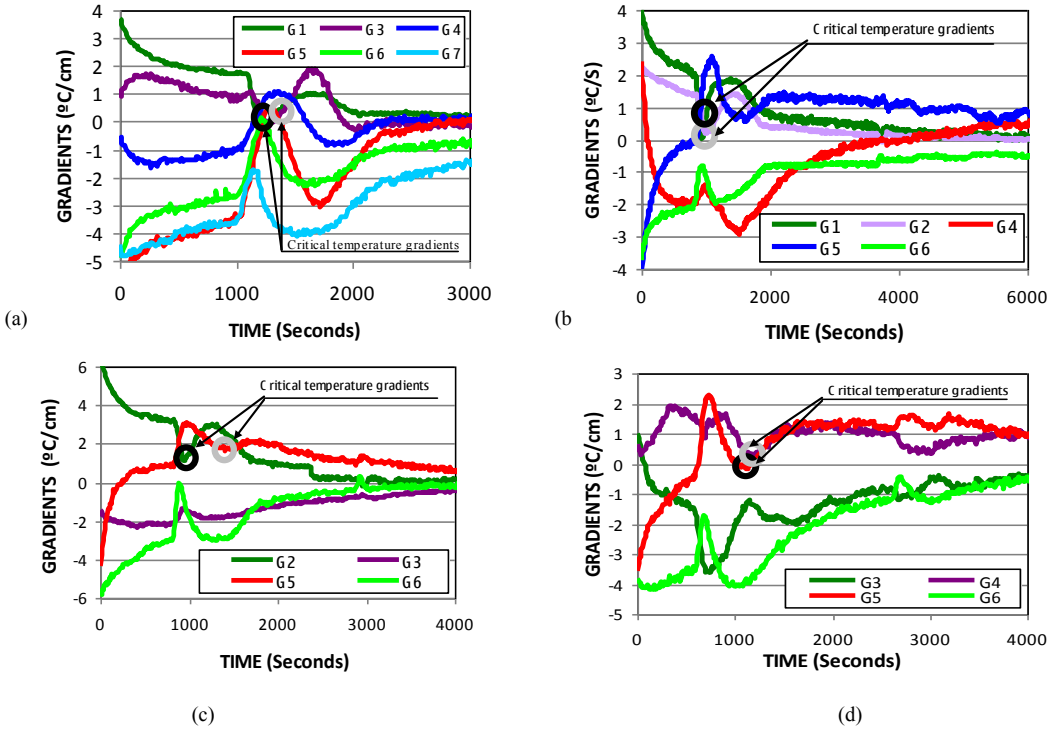

Fig. 6. Temperature gradient versus time: (a) Zn-4wt.%Sn, (b) Zn-6wt.%Sn, (c) Zn-10wt.%Sn, (d) Zn-30wt.%Sn alloys.

3.3. Secondary dendritic arm spacing (λ_2)

The secondary dendritic arm spacing was plotted as a function of distance for each sample in Figure 6 (a), (b), (c) and (d). In these figures it is observed that in all cases the size of the secondary spacing increases from both sides (columnar zones) and presents the maximum values in the central region of the samples (fully equiaxed zone).

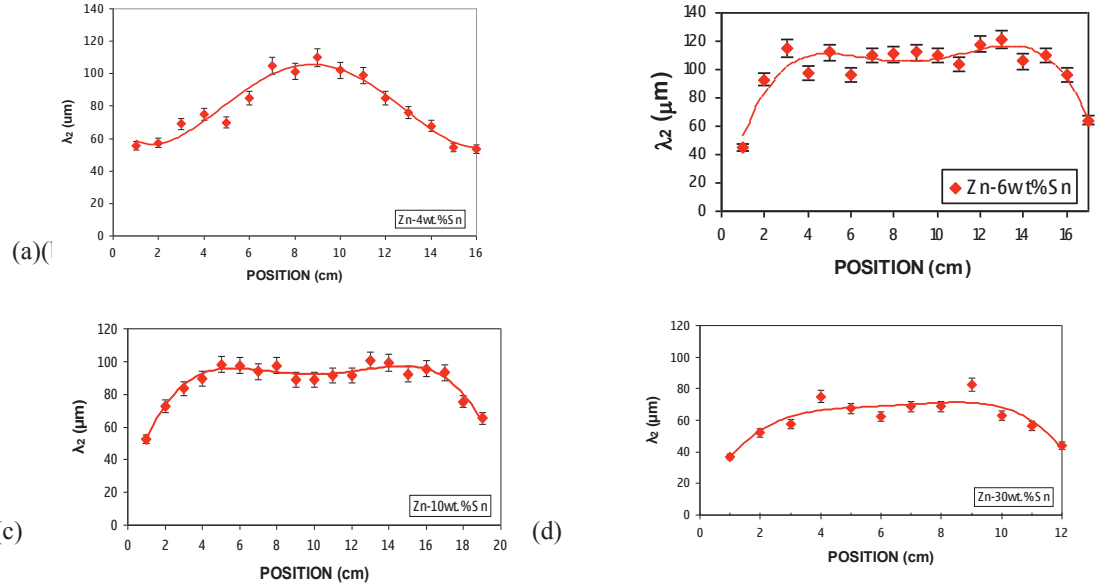

Fig. 7. Secondary dendritic arm spacing versus position: (a) Zn-4wt.%Sn, (b) Zn-6wt.%Sn, (c) Zn-10wt.%Sn, (d) Zn-30wt.%Sn alloys.

3.4. Secondary dendritic arm spacing (λ_2) versus local solidification time (t_{SL})

The main solidification parameters necessary for the analysis are the growth velocity (V) and the temperature gradient (G). They are calculated as:

$$V = \frac{2\ cm}{\Delta t}, \quad G = \frac{\Delta T}{2\ cm} \quad \text{and} \quad t_{SL} = \frac{\Delta T}{GV} \tag{1}$$

where Δt is the time taken for the inter-phase (liquid or solid) to pass two consecutive thermocouple positions, ΔT is the temperature difference between the same thermocouples and 2 cm is the separation distance between each pair of thermocouples. In general, the spacing and time have been related through an equation of type: $\lambda_2 = K_1 * t_{SL}^{\ a}$, where a and K_1 are parameters associated to the particular alloy system (Spittle 2006). In Figure 7 it can first be observed that in all cases, an increase in the local solidification time produces an increase in the secondary spacing. Moreover, it can be observed the relationship between λ_2 and t_{SL} for each alloy concentration. The parameter K1 increases with Sn content in the alloy and the constant a decreases from 4 wt.%Sn to 30wt.%Sn.

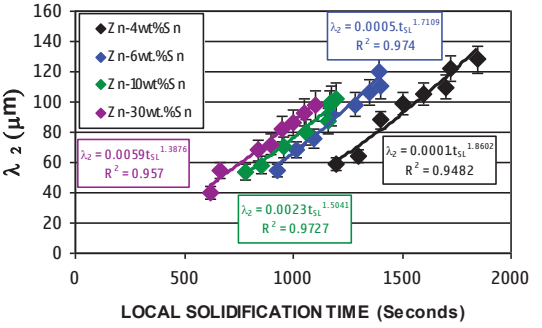

Fig. 8. Secondary dendritic arm spacing versus local solidification time.

4. Conclusions

The columnar-to-equiaxed transition (CET) was obtained in Zn-Al alloys horizontally directionally solidified in a rage of alloy concentrations between Zn-4wt.%Sn and Zn-30wt.%Sn. Also, the main parameters involved in the CET were determined. These parameters were: cooling rates, the average temperature gradients and critical temperature gradients at the CET, the local solidification time.

Secondary dendritic arm spacings increase from both sides of the samples to the centre and with an increase in the local solidification time.

Different expressions and values of constants correlating secondary dendritic arm spacing and local solidification time were obtained; it is important to note that constants of expressions change from alloy to alloy.

Acknowledgements

This work was partially supported by the Argentinean Research Council (CONICET) and the National Agency for Science and Technology (PICT-2011-1378).

References

Ares, A.E., Schvezov, C.E., Solidification Parameters during the Columnar-to-Equiaxed Transition in Lead-Tin Alloys. Metallurgical and Materials Transactions, 31A (2000) p.p. 1611-1625.

Ares, A.E., Gueijman, S.F., Schvezov, C.E., 2002. Semi-Empirical Modeling for Columnar and Equiaxed Growth of Alloys. J. Crystal Growth 241, 235-240.

Ares, A.E., Gueijman, S.F., Caram, R., Schvezov, C.E., 2005. Semi - Empirical Modeling for Columnar and Equiaxed Growth of Alloys. J. Cryst. Growth, 275, 319-325.

Ares, A. E., Schvezov, C. E., 2007. Influence of Solidification Thermal Parameters on the Columnar-to-Equiaxed Transition of Aluminum-Zinc and Zinc-AluminumAlloys. Metall. Mater. Trans. A 38, 1485-1499.

Ares, A. E., Schvezov, C. E., 2010. Experimental Study of the Columnar-to-Equiaxed Transition during Directional Solidifcation of Zinc-Aluminum Alloys and Composites. World Journal of Engineering.

Ares, A.E., Schvezov, C.E., 2013. Columnar-to-Equiaxed Transition in Metal-Matrix Composites Reinforced with Silicon Carbide Particles. Journal of Metallurgy. In Press.

Auras, R., Schvezov, C.E., 2004. Wear Behavior, Microstructure, and Dimensional Stability of As-Cast Zinc-Aluminum/SiC (Metal Matrix Composites) Alloys. Metallurgical and Materials Transactions A 35, 1579-1590.

Gandin, Ch.-A., 2000. Experimental Study of the Transition from Constrained to Unconstrained Growth During Directional Solidification. ISIJ International 40, 971-979.

Gandin, Ch. A., 2000, From Constrained to Unconstrained Growth During Directional Solidification. Acta Materialia 48, 2483-2501.

Gueijman, S. F., Schvezov, C. E., Ares, A. E., 2010. Directional Solidification and Characterization of Zn-Al and Zn-Ag Diluted Alloys. Materials Transactions 51, 1851-1870.

Hunt, J.D., 1984. Steady State Columnar and Equiaxed Growth of Dendrites and Eutectic. Mater. Sci. Eng. 65, 75-83.

Mahapatra, R.B., Weinberg, F., 1987. The Columnar to Equiaxed Transition in Tin-Lead Alloys. Metall. Trans. B 18, 425-432.

McFadden S., Browne D.J.,Gandin Ch.-A., 2009. A Comparison of CET Prediction Methods using Simulation of the Growing Columnar Front. Met. Mat. Trans. 40A, 662-672.

Moffatt, W.J. 1984. Handbook of Binary Phase Diagrams, Published by General Electric Company Corporate Research and Development Technology Marketing Operation, New York, p.p. 259, 419, 437, 391.

Reinhart, G., Mangelinck-Noël, N., Nguyen-Thi, H., Schenk, T., Gastaldi, J., Billia, B., Pino, P., Härtwig, J., Baruchel, J., 2005. Investigation of columnar-equiaxed transition and equiaxed growth of Aluminium based alloys by x-ray radiography. Materials Science and Engineering A 384, 413-414.

Spittle, J.E., 2006. Columnar-to-Equiaxed Grain Transition in as Solidified Alloys, International Materials Reviews 51, 247-269.

Vander Voort, G.F., 2000. In: Metallography Principles and Practice, ASM International, New York, p.p. 528-761.

Ziv, I., Weinberg, F., 1989. The Columnar-to-Equiaxed Transition in Al 3 Pct Cu. Metallurgical and Materials Transactions A 20, 731-734.